Quantitative Evaluation Of Actual Loss Reduction Benefits of a Renewable Heavy DG Distribution Network

Onyema S. Nduka and Bikash C. Pal, *Fellow, IEEE*

***Abstract*—Modern distribution network architectures have greatly changed due to the increasing proliferation of the network with power converters of renewable distributed generators (RDGs) and switching electronic loads. While these RDGs may offer benefits to the distribution network operator in terms ofnetwork loss reduction, the quantification of such benefits are usually investigated on the basis that harmonics from the power converters are negligible. In this paper, the electrical power losses in a network with significant penetration of photovoltaics (PVs) is assessed. The harmonics from the power conditioners of the PVs and network background distortions have been taken into account in the analysis. Technical insights from study of practical distribution networks are presented.**

***Index Terms*—Quantitative evaluation, loss reduction, distribution network, harmonics, advanced harmonic domain (AHD) frame of reference, distributed generation, power quality, modelling, harmonic analysis, harmonic load flows.**

NOMENCLATURE

CE	'Constitutive equation'.
VCE	'Voltage constitutive equation'.
Tx	Transformer.
PV	Photovoltaic.
P_{pv}, Q_{pv}	Real and reactive power of PV respectively.
S_{pv}	Apparent power of PV inverter.
V_{dc}	DC voltage from PV module (V).
LFA	Load flow analysis.
i	Imaginary term.
p	Number of pulses.
f, g	Nodes f and g respectively.
q	qth pulse index.
γ_q	Pulse switching pulse mid-point.
β_q	Pulse width.
θ	Angle in rads.
E_g	Grid voltage.
L_v	Inductance, $L_2 + L_g$.
DN	Distribution network.
HDECA	Harmonic domain extended computer aided.
CCE	'Current constitutive equation'.
i_c, V_c	Capacitor current and voltage respectively.
$G(\theta)$	Switching function.
$v(0^-)$	Initial capacitor voltage.
C	LCL filter capacitor.
L_1	LCL filter inductance on PV side.
PCC	Point of common coupling.
r, y, b	Red, yellow and blue -phase respectively.
i_{pcc}	Time domain PCC current.
AHD	Advanced harmonic domain.
$AHDRF$	AHD reference frame.
$[\mathbf{I_{pcc}}]$	AHD PCC current.
$[\mathcal{U}], [\mathbf{\Psi}]$	AHD identity and differentiation matrices respectively.
i_{pv}	Photovoltaic (PV) system current.
$[\mathbf{I_{pv}}]$	AHD coefficients of i_{pv}.
HN	Harmonic Norton.
$[\mathbf{Y_{hd}}]$	AHD-HN admittance matrix of PV.
$[\mathbf{I}]$	AHD-HN current source.
$[\mathbf{Y_{Aug}}]$	AHD Augmented admittance matrix.
$ECAHA$	Extended computer aided harmonic analysis.
$ECAHLFA$	Extended computer aided harmonic LFA.
$[\xi]$	ECAHA solution variables.
$[\mathbf{J}]$	Vector of current and voltage sources.
$[\Omega]$	Vector of non-linear functions.
$[\mathbf{Y_{cap}}]$	AHD admittance matrix of shunt capacitors.
$[\mathbf{Y_{ll}}]$	AHD admittance matrix of impedance loads.
$[\mathbf{C}], [\mathbf{\Gamma}], [\mathbf{Z}]$	Generalized augmentation matrices in AHDRF.
ΔP_{Fdr}	Total feeder losses (kW).
NF	Number of feeders.
σ	Phase index.
nf	Feeder index.
I_{Fdr}, R_{Fdr}	Feeder current and resistance.
RPF	Reverse power flow.
NLL	Nonlinear load.

Manuscript received June 1, 2017; revised October 10, 2017; accepted November 19, 2017. Date of publication December 19, 2017; date of current version June 18, 2018. This work was supported in part by the Engineering and Physical Sciences Research Council (EPSRC) UK under the Reliable and Efficient System for Community Energy Solution RESCUES Grant EP/K03619X/1 and in part by the Federal Government of Nigeria through the Petroleum Technology Development Fund and Presidential Special Scholarship for Innovation and Development. Paper no. TSTE-00509-2017. *(Corresponding author: Bikash Chandra Pal.)*

O. S. Nduka is with the Control and Power Research Group, Electrical and Electronic Engineering Department, Imperial College, London SW7 2AZ, U.K., and also with the Federal University of Technology, Owerri 1526, Nigeria (e-mail: on212@ic.ac.uk).

B. C. Pal is with the Control and Power Research Group, Electrical and Electronic Engineering Department, Imperial College, London SW7 2AZ, U.K. (e-mail: b.pal@imperial.ac.uk).

Color versions of one or more of the figures in this paper are available online at http://ieeexplore.ieee.org.

Digital Object Identifier 10.1109/TSTE.2017.2776610

THD	Total harmonic distortion.
rms	Root mean square.
MNA	Modified nodal analysis.

I. Introduction

RESEARCH has shown that electrical losses will increase in future power networks [1]. This has been attributed to increased demand, stray losses, line congestion, network and load imbalance, harmonic pollution, reverse power flows (RPF) and voltage rise due to intermittent generation from renewable distributed generators (RDGs). These losses have been categorized into two broad groups namely: technical and non-technical losses [2], [3]. Technical losses occur due to the currents flowing through the lines/feeders, transformers etc, to supply the loads and are further classified as load and no-load technical losses. While the load losses depend on the loading level, the no-load technical losses is unaffected by network load. As a result, load and no-load technical losses are respectively termed copper and iron losses in the literature [4], [5].

The losses in the network are useful indicators for assessing the power delivery efficiency of a utility. Hence, this area of technical work has attracted the attention of several utilities and researchers. Traditionally, network losses have being evaluated from load flow analysis (LFA) simulations. For such analysis, the current injection method, forward backward sweep [6] and optimisation based methods are well understood in the power systems literature [7]. The solution variables from the above techniques are post-processed to obtain the network loss values.

Furthermore, several techniques used for network loss reduction exist in the literature such as: replacement of old utility equipment, re-conductoring, network re-configuration, optimal deployment of RDGs and load balancing [4]. Of these techniques, the use of RDGs is gaining unprecedented interests due to the quest for greener and emission free electricity sources.

Amidst the RDGs deployed for power generation, rooftop PVs are highly favourable at the consumer level. The benefits of these RDGs such as voltage profile improvement, frequency and reactive power support, network loss reduction, transformer and feeder loading stress reduction have been proven at the fundamental frequency in the power system literature. It is also well-known that the location and sizing of these RDGs impact the benefits that accrue from them [8].

This paradigm shift in the architecture of modern power networks due to integration of renewable energy resources are not without technical and operational challenges to the utility's system. For instance, the RDGs require power converters for interfacing to the grid. Such converters are sources of harmonic pollution [9]. In addition to harmonics, RPF and voltage rise issues have been identified as two major challenges which exist in networks with high penetration of PV-RDGs. Nevertheless, the use of intelligent inverters and storage systems can be used to control the power flows between the grid and the PV systems and hence mitigate voltage rise.

Indeed, the benefits and challenges relating to RDGS are often quantified with reference to the fundamental frequency alone. The harmonics generated from the power converters of the PV-RDGs and network operating conditions like unbalance are usually neglected. In fact, it has been reported that harmonics and unbalance problems can occur due to significant uptake of PVs [10], [11].

It is obvious that few PV-RDGs integrated into the utility network will not pose any significant operating challenges in terms of harmonics and unbalance. Rather, they can be optimally operated to reduce the customer demand on the feeder. However, with the proliferation of RDGs (in addition to other switching loads) in the modern power grid, it is necessary to re-quantify the benefits of RDGs - especially in terms of network loss reduction. This assessment must include the non-fundamental (harmonics) frequency voltages and currents generated by the RDG power conditioners, background distortions and unbalanced loading. This is vital given that increase in penetration level of these units can alter the harmonic emission levels and unbalance of the system and thus influence the network losses.

Consequently, it is useful to establish how PV clusters will perform with respect to loss reduction for networks with significant background distortions and unbalanced network condition. This will justify the use of RDG integration over traditional disruptive techniques for loss reduction.

Furthermore, as have been established in the literature [12], [13], the harmonic performance of RDGs is influenced by the network operating conditions. This is however, less likely when robust controllers and harmonic compensators are deployed [14]. Such complex controllers are able to reject network background harmonics and unbalance effects on the PV system performance. The use of such control schemes will however increase the complexity and cost of the PV units. As a result, the use of simple controllers is often considered as a trade-off between robust disturbance rejection and the economics of the control scheme. This compromise results in a higher (than expected) harmonics generations from the PV-RDGs.

As mentioned earlier, while few PV-RDG units integration do not cause network operational issues, the collective contributions from several units could pose technical difficulties to utility system. This therefore has created doubts among some utilities in the accommodation of significant uptake of RDGs such as PV clusters [15]. On the other hand, such neglect to integrate high penetration of PV-RDGs into the system will deprive utilities of other ancillary support services (such as substation loading relief) that could be obtained from such low carbon technologies (LCTs).

It is pertinent to mention that several efforts have been made by previous researchers in the area of investigation of harmonics losses. In [16] and [17], simple harmonics loss calculation methods using voltage and current total harmonics distortions (THDs) have been proposed. The rms and THD values of voltages and currents were obtained from measurements. The study focused on typical nonlinear devices in residential and commercial buildings such as computers, TVs, referigerators and air-conditioners. Typical urban networks investigated by [16] revealed that losses due to harmonics were significant. Large tripplen harmonics were noticed in the current measurements of the neutral conductors. The study in [16] however, neglected skin effect in the conductor resistances as well as background

voltage harmonics distortion. That study was limited to the LV side of the distribution transformer. Typical features of distribution systems (e.g. unbalance and untransposed lines) were not considered. This is similar to [17] which assumed balanced 3-phase system. Moreover, neither of the above studies included PV clusters in their analysis.

Another study in [18] has also investigated harmonics losses in a medium voltage distribution system in South Africa. Using the currents and voltage THDs obtained from measurements in the network, the authors estimated other values of current THDs based on a regression formula which expressed the current THD as a function of the voltage THD. The newly estimated current THDs were used to evaluate harmonics loss contributions. While authors claimed that the test network had infinitesimally small harmonics loss impacts, it suggested that possible increase in harmonics emission levels would necessitate system upgrade. That is especially for DNs that were planned without considering harmonics. The use of regression formula between current THD and voltage THD may however be affected by measurement noise in the data. It is also possible that the dependence of other NLL output harmonics currents on voltage background distortions may not have been fully captured at the instance of measurements. No detailed considerations were given to unbalanced harmonics, mutually-coupled and untransposed lines; therefore, possible phase couplings and associated losses might have been neglected. In fact, analysis using measurement data need to be validated with detailed network assessment. Moreover, that study did not include the PV-RDGs impacts in relation to harmonics and unbalanced induced losses.

Indeed, it has been suggested that the use of the traditional THD voltage and current expressions do not reflect accurate loss estimates for unbalanced 3-phase non-sinusoidal operating conditions in the distribution systems. One major reason for this is that the well-known THD expression for either voltage or current is usually a ratio with respect to single phase fundamental frequency voltage or current. As a result, phase couplings, unbalanced harmonics and neutral currents (including harmonics currents) are often neglected [19].

Furthermore, the above previous studies have used phasor domain (decoupled) techniques in their analysis. This decoupling downplays the interaction between fundamental and harmonic frequencies. This interaction between harmonic frequencies occur due to nonlinearities (for instance power converter switching and transformer saturation) [20].

To deal with all harmonics existing in a given system simultaneously, a frame of reference called the 'harmonic domain' was proposed in [21]. This method analyzes the harmonics present in the network as vectors in n-dimensional plane. This is unlike the phasor analysis which projects all the harmonic components onto a single plane. This reference frame which is capable of assessing the harmonic cross-couplings have been used by different authors including [20] and [22].

In [20], harmonic power flows formulated based on the instantaneous power conservation principle was proposed. The test system studied was a transmission network. Due to the complexity of the method, the test network used was a simple balanced 3-node system with a single harmonics source - thyristor controlled reactor. Therefore, only single-phase analysis was presented. Also, the linear load models (constant power models) used do not accurately capture the performance of aggregated linear loads at harmonic frequencies. This is especially for motor loads. Constant power motor load models do not reflect the actual unbalance voltage levels which exist in most 3-phase networks [23]. A further detailed insight into harmonic load model for aggregated linear loads can be found in [24].

In [22], the authors applied the AHD technique for calculating the rms voltages and currents for a test transmission network. The AHD was combined with the MNA approach. Apart from studying a transmission system, PV-RDG clusters were not investigated in that study. Also, assessment of harmonics induced losses was outside the scope of that work.

Furthermore, in [25], the harmonics losses associated with significant penetration of compact fluorescent lamps have been presented. Authors employed the harmonic Norton approach (based on measurements) in the analysis. The study assumed balanced 3-phase system and therefore ignored typical characteristics of DNs. Also PV-RDG clusters were not considered.

In this paper, for the first time (to authors best knowledge), a detailed quantitative evaluation of the performance of PV-RDG clusters in reducing DN feeder losses in the face of background harmonics distortion and network unbalance is investigated. The study presented in this paper also takes into account the harmonics associated with the PV power conditioners. Truly, the detailed harmonics loss analysis became pertinent following the 'innovation challenge call' by a UK-DNO which suggested the need for technical innovations in this area of power systems specialism - harmonics and its impacts on network losses [26].

This study was also motivated by the increased number of field trials currently being performed by UK-DNOs [27], [28] to better understand the impacts (e.g. harmonics) due to significant LCT (e.g. distributed PV) uptake on the network. Also, utilities wish to know if there exists business case for leveraging on these LCTs to optimize network performance (including loss reduction). When fully proven, such LCT uptake rather than the classical disruptive technologies such as transformer replacement will be used to improve system performance.

Similar to [22], the extended MNA formulated in AHD frame of reference has been used in this study. In this way, typical characteristics of DNs such as load unbalance, mutually coupled and untransposed lines and unbalanced harmonics have been included in the analysis. All harmonics have also been considered simultaneously - an advantage of the AHD reference frame. However, unlike [22], this technical work focuses on PV-RDG clusters, their harmonics and unbalance impacts and the evaluation of actual loss reduction benefits from significant uptake of such LCTs in the DN. Such PV-RDG clusters are found at social housing and commercial buildings (like schools and office complex) in the UK [28] and in Nigeria.

Two practical test DNs have been considered in the analysis in this paper - UKGDS 95 bus model and modified IEEE-13 bus (highly unbalanced) distribution systems. For the purpose of comparative evaluation between fundamental and harmonics induced losses, the analysis and simulations implemented are scenario based. Hence, four scenarios have been studied viz: net-

work operating - without background harmonics and PV-RDGs, with background harmonic distortions but no PV-RDGs, with PV-RDGs acting as generators only at fundamental frequency, and the case of PV-RDGs supplying currents at both fundamental and harmonic frequencies and in the presence of network background distortions. The results of the different scenarios are discussed for a useful technical insight.

II. Harmonic Domain Extended Computer Aided Analysis (HDECAA) of the Distribution Network

Distribution systems generally have operating conditions that are different from transmission networks. Consequently, the use of symmetrical component modelling approach does not offer any benefit for distribution system analysis [23]. Indeed, phase frame modelling approach has been proposed for distribution system analysis [23]. Therefore, DN components like transformers, capacitors, switches etc. have been modelled in detail using the phase-frame approach in the AHD reference frame.

A. HDECA Single Phase PV Modelling

A PV-RDG is often modelled as constant power (PQ) or generator (PV) node in classical LFA. The PQ values are either measured or estimated using established deterministic or probabilistic equations [29]. Such modelling neglects the harmonic currents and voltages generated by the power conditioning unit of the PV-RDG. Consequently, the current provided by the PV system can be computed viz:

$$I_{pv} = \left(\frac{P_{pv} + jQ_{pv}}{V_g} \right)^* \tag{1}$$

where P_{pv} and Q_{pv} are the estimated real and reactive powers of the PV units. V_g is the terminal voltage at the point of PV connection. Since the P_{pv} values are often available (by estimation or measurements), thus Q_{pv} can be obtained using the formula below:

$$Q_{pv} = \sqrt{(S_{pv}^2 - P_{pv}^2)} \tag{2}$$

where S_{pv} is the apparent power of the inverter unit (kVA). The above equations hold true on the assumption that the inverter unit is not over-rated. While this model is reasonable for networks with few PV units and negligible network background harmonic distortion, a significant penetration of switching elements would require that the harmonic contents of the voltages and currents from the power converters be included in the analysis.

In general, a PV-RDG essentially consists of a direct current (dc) voltage source (PV panels or modules), inverter-, filtering -, control- and protective circuits. A micro-controller based converter programmed using the harmonic elimination concept can be modelled by using switching functions as shown in [12]. This paper deploys a simplified version of the single-phase PV system of [12] for the analysis presented in this work. The equations of this PV model have been written in this paper for the purpose of completeness. The ac voltage can be related to the dc via (3).

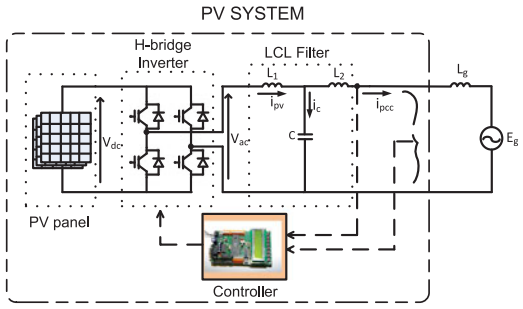

Fig. 1. Single phase PV system simplified diagram.

$$V_{ac}(\theta) = -\left(\sum_{k=-\infty}^{\infty} \frac{i4}{\pi} \left(\sum_{q=1}^{p} \frac{1}{k} \sin\left(k\gamma_q\right) \sin\left(\frac{k}{2}\beta_q\right) \right) \times \exp(ik\theta) \right) V_{dc} \tag{3}$$

where k, q, γ_q, β_q denote the kth harmonic, pulse index of switching function, switching pulse mid-point and pulse width respectively. Also the term $\theta = \omega t$. The circuit diagram of Fig. 1 can be used to derive the Norton equivalent circuit in the AHD.

$$E_g(t) - V_c(t) + L_v \frac{di_{pcc}(t)}{dt} = 0 \tag{4}$$

$$G(\theta)V_{dc} - V_c(t) - L_1\left(\frac{di_c(t)}{dt} + \frac{di_{pcc}(t)}{dt} \right) = 0 \tag{5}$$

$$V_c(t) - \frac{1}{C}\int i_c(t)dt - v(0^-) = 0 \tag{6}$$

where

$$G(\theta) = -\left(\sum_{k=-\infty}^{\infty} \frac{i4}{\pi} \left(\sum_{q=1}^{p} \frac{1}{k} \sin(k\gamma_q) \sin\left(\frac{k}{2}\beta_q\right) \right) \times \exp(ik\theta) \right) \tag{7}$$

The terms $i_c(t)$, $V_c(t)$ and $i_{pcc}(t)$ are respectively the filter capacitor - current and voltage and the current injected into the grid. Consider that the above signals (e.g. $E_g(t)$) are time-periodic and satisfy Jordan Dirichlet's condition; thus can be expressed as Fourier series. Then, as an illustration,

$$E_g(t) = \sum_{h=-\infty}^{\infty} E(h)\exp(ih\omega t) \tag{8}$$

This transforms into the AHD as:

$$E_g(t) = \beta(t)\mathbf{E} \tag{9}$$

where for a truncated Fourier series,

$$\beta^{\mathbf{T}}(t) = \begin{vmatrix} \exp(-iH\omega t) \\ \exp(i(1-H)\omega t) \\ \vdots \\ 1 \\ \vdots \\ \exp(i(H-1)\omega t) \\ \exp(iH\omega t) \end{vmatrix}; \mathbf{E} = \begin{vmatrix} E(-H) \\ E(1-H) \\ \vdots \\ E(0) \\ \vdots \\ E(H-1) \\ E(H) \end{vmatrix} \tag{10}$$

Based on the substitution of terms into (4), (5) and (6), the following expressions are realized:

$$\sum_{h=-\infty}^{\infty} E(h)\exp(ih\omega t) - \sum_{r=-\infty}^{\infty} V_c(r)\exp(ir\omega t) + L_v\frac{d}{dt}\sum_{m=-\infty}^{\infty} I_{pcc}(m)\exp(im\omega t) = [0] \tag{11}$$

$$-\left(\sum_{k=-\infty}^{\infty}\frac{i4}{\pi}\left(\sum_{q=1}^{p}\frac{1}{k}\sin\left(k\gamma_q\right)\sin\left(\frac{k}{2}\beta_q\right)\right)\times\exp(ik\theta)\right)V_{dc} - \sum_{r=-\infty}^{\infty} V_c(r)\exp(ir\omega t) - L_1\frac{d}{dt}\sum_{y=-\infty}^{\infty} I_c(y)\exp(iy\omega t) - L_1\frac{d}{dt}\sum_{m=-\infty}^{\infty} I_{pcc}(m)\exp(im\omega t) = [0] \tag{12}$$

$$\sum_{r=-\infty}^{\infty} V_c(r)\exp(ir\omega t) - \frac{1}{C}\int\sum_{y=-\infty}^{\infty} I_c(y)\times\exp(iy\omega t) - [v(0^-)] = [0] \tag{13}$$

The expressions - (11), (12) and (13) are rewritten in the form of (9). Thereafter, matrix-vector algebra manipulations (in addition to harmonics balance conservation principle) are applied to obtain the AHD transformation as thus:

$$\mathbf{V_c} = \left([\mho] + L_1C[\mathbf{\Psi^2}] + \kappa[\mho]\right)^{-1}\left([\mathbf{G}]\mathbf{V_{dc}} + \kappa[\mho]\mathbf{E_g}\right) \tag{14}$$

$$\mathbf{I_{pcc}} = \frac{1}{L_v}[\mathbf{\Psi}]^{-1}[\mathbf{SSO}]^{-1}[\mathbf{G}]\mathbf{V_{dc}} + [\mathbf{\Psi}]^{-1}\left(\frac{\kappa}{L_v}[\mathbf{SSO}]^{-1} - \frac{1}{L_v}[\mho]\right)\mathbf{E_g} \tag{15}$$

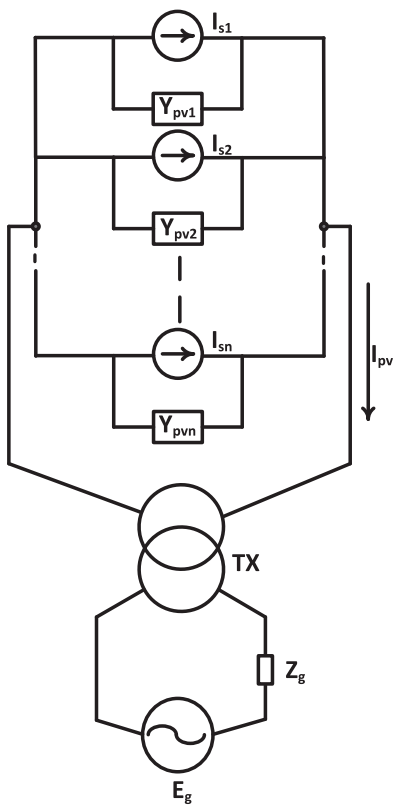

Fig. 2. Parallel connected single-phase PV system advanced HD equivalent circuit.

where

$$\kappa = \frac{L_1}{L_v}; [\mathbf{SSO}] = \left[\left(\frac{L_1+L_v}{L_v}\right)\mho + L_1C[\mathbf{\Psi^2}]\right] \tag{16}$$

$$\mathbf{I_{pv}} = \frac{1}{L_1}[\mathbf{\Psi}]^{-1}\left([\mho] - [\mathbf{SSO}]^{-1}\right)[\mathbf{G}]\mathbf{V_{dc}} - \left(\frac{1}{L_v}[\mathbf{\Psi}]^{-1}[\mathbf{SSO}]^{-1}\right)\mathbf{E_g} \tag{17}$$

$[\mho]$ and $[\mathbf{\Psi}]$ are respectively AHD identity and differentiation matrices. The expression (17) can be rewritten as (18).

$$\mathbf{I_{pv}} = \mathbf{I} + [\mathbf{Y_{hd}}]\mathbf{E_g} \tag{18}$$

where:

$$\mathbf{I} = \frac{1}{L_1}[\mathbf{\Psi}]^{-1}\left([\mho] - [\mathbf{SSO}]^{-1}\right)[\mathbf{G}]\mathbf{V_{dc}} \tag{19}$$

$$[\mathbf{Y_{hd}}] = -\left(\frac{1}{L_v}[\mathbf{\Psi}]^{-1}[\mathbf{SSO}]^{-1}\right) \tag{20}$$

Often, multiple single phase PV-RDGs are connected in parallel at the same PCC. Such arrangement can be modelled based on the equivalent circuit of Fig. 2. To reduce system model complexity, it is assumed that all single-phase paralleled PV-RDGs are operating under the same conditions. Consequently, the harmonic coefficients of net current injection from PV-RDG cluster $\mathbf{I_{pv,net}}$ can be written as (21).

$$\mathbf{I_{pv,net}} = \mathbf{I_{pv1}} + \mathbf{I_{pv2}} + \cdots + \mathbf{I_{pvn}} \tag{21}$$

The time domain current expression can be written namely:

$$\mathbf{I_{PV,cluster}}(t) = \beta(\mathbf{t})\mathbf{I_{pv,net}} \tag{22}$$

where:

$$\mathbf{I_{pv,net}} = \begin{vmatrix} I_{pv,net}(-H) \\ I_{pv,net}(1-H) \\ \vdots \\ I_{pv,net}(0) \\ \vdots \\ I_{pv,net}(H-1) \\ I_{pv,net}(H) \end{vmatrix} \tag{23}$$

Also, the AHD coefficients of the cluster PV-RDG admittances, $[Y_{pv,net}]$, is as provided in (24).

$$[\mathbf{Y_{pv,net}}] = [\mathbf{Y_{pv1}}] + [\mathbf{Y_{pv2}}] + \cdots + [\mathbf{Y_{pvn}}] \tag{24}$$

The single-phase PV data used for simulation have been obtained from [30].

III. ECAHA Network Equation Formulation

The extended computer aided harmonic load flow analysis (ECAHLFA) approach models the power network in steady state as in (25).

$$[W(\xi)] = [\mathbf{Y_{Aug}}][\xi] + [\mathbf{\Omega}] + [\mathbf{J}] = [\mathbf{0}] \tag{25}$$

where

$$[\xi] = \left|\begin{array}{c} [\mathbf{V_1}] \\ [\mathbf{V_2}] \\ \vdots \\ [\mathbf{V_n}] \\ \hline [\mathbf{I_{x_1}}] \\ [\mathbf{I_{x_2}}] \\ \vdots \\ [\mathbf{I_{x_p}}] \end{array}\right|;\ [\mathbf{J}] = \left|\begin{array}{c} [\mathbf{I_1}] \\ [\mathbf{I_2}] \\ \vdots \\ [\mathbf{I_n}] \\ \hline [\mathbf{V_{x_1}}] \\ [\mathbf{V_{x_2}}] \\ \vdots \\ [\mathbf{V_{x_p}}] \end{array}\right| \tag{26}$$

The terms $[\xi]$, $[\Omega]$ indicate the system solution variables and the set of nonlinear equations for the switching electronic elements. The system variables are voltages and selected current variables. [J] denotes the vector of independent current and voltage sources. The indexes 'n' and 'p' in (26) are respectively the total number of nodes and number of selected 'non-natural elements' [31] currents included in system model equations. The 'non-natural elements' are network devices whose currents cannot be easily expressed in terms of their admittance matrices; for example switches. The subscript 'x' is used to denote the independent voltage- or current- sources. It is important to note that each variable in (26) above has been written with respect to the AHD reference frame. That is for instance, consider the voltage of phase 'r', then

$$[\mathbf{V_e^r}]^T = \left| V_e^r(-h)\ V_e^r(1-h)\ \cdots\ V_e^r(h-1)\ V_e^r(h) \right| \tag{27}$$

where: $e \in \{1, 2, 3, 4, \cdots, n\}$

For a 3-phase system with phases 'r', 'y' and 'b', the voltage expression for node 'e' is provided in (28).

$$\left|\begin{array}{c} [\mathbf{V_e^r}] \\ \hline [\mathbf{V_e^y}] \\ \hline [\mathbf{V_e^b}] \end{array}\right| = \left|\begin{array}{c} \mathbf{V_e^r}(-\mathbf{K}) \\ \mathbf{V_e^r}(-K+1) \\ \vdots \\ \mathbf{V_e^r}(K-1) \\ \mathbf{V_e^r}(K) \\ \hline \mathbf{V_e^y}(-K) \\ \mathbf{V_e^y}(-K+1) \\ \vdots \\ \mathbf{V_e^y}(K-1) \\ \mathbf{V_e^y}(K) \\ \hline \mathbf{V_e^b}(-K) \\ \mathbf{V_e^b}(-K+1) \\ \vdots \\ \mathbf{V_e^b}(K-1) \\ \mathbf{V_e^b}(K) \end{array}\right| \epsilon \mathbb{C}^{(6H+3)\times 1} \tag{28}$$

With loads treated as constant impedance loads at the fundamental frequency and using non-fundamental frequency load models proposed in [24] for the harmonic case, the expression (25) translates to a set of algebraic equations in the AHD. As a result, the ECAHLFA is reduced to the extended computer aided harmonic analysis (ECAHA). The AHD solution variable to be computed is $[\xi]$ which is defined in (26). The resulting equation to be solved is as given in (29).

$$\left[\begin{array}{c|c} [\mathbf{Y}] & [\mathbf{C}] \\ \hline [\mathbf{\Gamma}] & [\mathbf{Z}] \end{array}\right] \left|\begin{array}{c} [\xi_{\mathbf{V}}] \\ \hline [\xi_{\mathbf{I}}] \end{array}\right| - \left|\begin{array}{c} [\mathbf{J_I}] \\ \hline [\mathbf{J_V}] \end{array}\right| = \left|\begin{array}{c} [\mathbf{0}] \\ \hline [\mathbf{0}] \end{array}\right| \tag{29}$$

$$[\mathbf{Y}] = [\mathbf{Y_{line}}] + [\mathbf{Y_{cap}}] + [\mathbf{Y_{ll,load}}] \tag{30}$$

For 3-phase ECAHA, the line elements were obtained using Dubanton's equations (a closed form approximation of the Carson's equations). This is as presented below for two adjacent conductors - g and f [32]:

$$Z_{geo}^{gg} = \frac{i500}{\pi}\omega\mu_0 \ln\left(\frac{2(h_g+\rho)}{r_{e,g}}\right)\Omega/\text{km} \tag{31}$$

$$Z_{geo}^{gf} = \frac{i500\omega\mu_0}{\pi} \ln\sqrt{\left(\frac{\Xi + (h_g+h_f+2\rho)^2}{d_{gf}^2}\right)}\Omega/\text{ km} \tag{32}$$

$$\Xi = \left(L_g^2 - 2L_fL_g + L_f^2\right) \tag{33}$$

$$d_{gf}^2 = (h_g - h_f)^2 + (L_f - L_g)^2\ \text{m}^2 \tag{34}$$

$$\rho = \frac{1}{\sqrt{i\omega\mu_0\sigma}};\quad \mu_0 = 4\pi \times 10^{-7}\ \text{H/m} \tag{35}$$

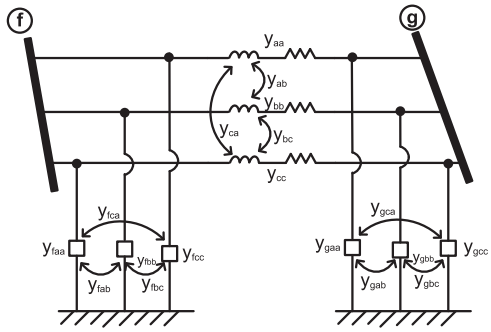

Fig. 3. 2-node distribution line.

Note that σ, μ_0 and ρ represent respectively the earth conductivity (in S/m), permeability of free space (in H/m) and the complex depth. The h and L terms represent height above ground and horizontal distance between conductors. Also, r_e and r_i respectively denote the external and internal resistances of conductors.

The impedance of the skin effect is:

$$Z_{sk} = \sqrt{R_0^2 + z_\infty} \quad \Omega/\text{km} \tag{36}$$

where:

$$R_0 = \frac{1}{\pi(r_{e,g}^2 - r_{i,g}^2)\sigma}; \quad z_\infty = \frac{1}{2\pi r_{e,g}\sigma\rho} \tag{37}$$

The impedance is the sum of the geometric impedance (Z_{geo}) and impedance due to skin effect (Z_{sk}). The impedance of the line at the hth harmonic frequency is arranged in the form of (38):

$$[Z_{abc}(h)] = \begin{bmatrix} Z_{aa} & Z_{ab} & Z_{ac} \\ Z_{ba} & Z_{bb} & Z_{bc} \\ Z_{ca} & Z_{cb} & Z_{cc} \end{bmatrix}(h) \tag{38}$$

The reciprocal of the impedance of the line i.e. (38) yields the admittance matrix of the line at that harmonic frequency. The mutually coupled and untransposed 2-node distribution line is as illustrated in Fig. 3. Since lines are considered as 'natural' elements, they are directly 'stamped' into the un-augmented admittance matrix - $[\mathbf{Y}]$ of (29). The line admittance expressed in the AHD reference frame is given as (39).

$$[\mathbf{Y_{line}}] = \begin{bmatrix} \ddots & & & \\ & [\mathbf{Y_{ff}}] & \cdots & [\mathbf{Y_{fg}}] \\ & \vdots & \vdots & \vdots \\ & [\mathbf{Y_{gf}}] & \cdots & [\mathbf{Y_{gg}}] \\ & & & \ddots \end{bmatrix}_{\mathbf{line}} \tag{39}$$

where for instance:

$$[\mathbf{Y_{xx}}] = \begin{bmatrix} [\mathbf{Y_{xx}^{rr}}] & [\mathbf{Y_{xx}^{ry}}] & [\mathbf{Y_{xx}^{rb}}] \\ [\mathbf{Y_{xx}^{yr}}] & [\mathbf{Y_{xx}^{yy}}] & [\mathbf{Y_{xx}^{yb}}] \\ [\mathbf{Y_{xx}^{br}}] & [\mathbf{Y_{xx}^{by}}] & [\mathbf{Y_{xx}^{bb}}] \end{bmatrix} \epsilon\, \mathbb{C}^{(6H+3)\times(6H+3)} \tag{40}$$

$$[\mathbf{Y_{xx}^{ts}}] = \begin{bmatrix} \ddots & & & \\ & [Y_{xx}^{ts}(-h,-k)] & \cdots & [Y_{xx}^{ts}(-h,k)] \\ & \vdots & \vdots & \vdots \\ & [Y_{xx}^{ts}(h,-k)] & \cdots & [Y_{xx}^{ts}(h,k)] \\ & & & \ddots \end{bmatrix} \tag{41}$$

$\{xx\} \epsilon \{ff, fg, gf, gg\}$ and $\{ts\} \epsilon \{rr, ry, \ldots, bb\}$; while h and k are the harmonic orders.

A condensed form of equation of (29) is as given in (42).

$$[\mathbf{Y_{Aug}}]\,[\xi] - [\mathbf{J}] = [\mathbf{0}] \tag{42}$$

where the augmented matrix $[\mathbf{Y_{Aug}}]$ is:

$$[\mathbf{Y_{Aug}}] = \left[\begin{array}{c|c} [\mathbf{Y_{line}}] + [\mathbf{Y_{cap}}] + [\mathbf{Y_{ll,load}}] & [\mathbf{C}] \\ \hline [\mathbf{\Gamma}] & [\mathbf{Z}] \end{array}\right] \tag{43}$$

$$[\xi] = \left|\begin{array}{c} [\xi_{\mathbf{V}}] \\ \hline [\xi_{\mathbf{I}}] \end{array}\right|; [\mathbf{J}] = \left|\begin{array}{c} [\mathbf{J_I}] \\ \hline [\mathbf{J_V}] \end{array}\right| \tag{44}$$

$[\mathbf{C}]$, $[\mathbf{\Gamma}]$ and $[\mathbf{Z}]$ are block matrices from the current and voltage expressions of the 'non-natural' devices. A generic expanded expression for the augmented admittance matrix $[\mathbf{Y_{Aug}}]$ is shown in (45).

$$[\mathbf{Y_{Aug}}] = \left[\begin{array}{cccc|c} \ddots & & & & \vdots \\ & [\mathbf{Y_{ff}}] & \ldots & [\mathbf{Y_{fg}}] & [\mathbf{C_f}] \\ & \vdots & \vdots & \vdots & \vdots \\ & [\mathbf{Y_{gf}}] & \ldots & [\mathbf{Y_{gg}}] & [\mathbf{C_g}] \\ & & & \ddots & \vdots \\ \hline \ldots & [\mathbf{\Gamma_f}] & \ldots & [\mathbf{\Gamma_g}] \ \ldots & [\mathbf{Z_t}] \end{array}\right] \tag{45}$$

For the purpose of clarity, the sub-matrices for non-natural elements is shown. For simplicity, consider only the electrical part model of a three single-phase transformer bank connected in delta-gounded wye arrangement. Then, the voltage descriptive equations (VDEs) can be derived by applying traditional circuit analysis. For this transformer connection, the voltage equation of (46) was derived.

$$[\mathbf{\Gamma_f}][\mathbf{V_f}] + [\mathbf{\Gamma_g}][\mathbf{V_g}] + [\mathbf{\Gamma_g}][\mathbf{Z_{tx}}][\mathbf{B_{tx}}][\mathbf{I_{tx}}] = [\mathbf{0}] \tag{46}$$

where:

$$[\mathbf{\Gamma_f}] = \begin{bmatrix} [\mho] & -[\mho] & \\ & [\mho] & -[\mho] \\ -[\mho] & & [\mho] \end{bmatrix}; [\mathbf{I_{tx}}] = \begin{vmatrix} [\mathbf{I_{tx}^{ry}}] \\ [\mathbf{I_{tx}^{yb}}] \\ [\mathbf{I_{tx}^{br}}] \end{vmatrix} \tag{47}$$

$$[\mathbf{\Gamma_g}] = -\begin{bmatrix} [\lambda_r \mho] & & \\ & [\lambda_y \mho] & \\ & & [\lambda_b \mho] \end{bmatrix}; \quad [\mathbf{B_{tx}}] = -[\mathbf{\Gamma_g}] \tag{48}$$

$$[\mathbf{Z_{tx}}] = \begin{bmatrix} [\mathbf{Z_{tx}^{rr}}] & [\mathbf{Z_{tx}^{ry}}] & [\mathbf{Z_{tx}^{rb}}] \\ [\mathbf{Z_{tx}^{yr}}] & [\mathbf{Z_{tx}^{yy}}] & [\mathbf{Z_{tx}^{yb}}] \\ [\mathbf{Z_{tx}^{br}}] & [\mathbf{Z_{tx}^{by}}] & [\mathbf{Z_{tx}^{bb}}] \end{bmatrix} \tag{49}$$

and

$$[\mathbf{Z_{tx}^{rr}}] = \begin{bmatrix} \ddots & & & \\ & [Z_{tx}^{rr}(-h,-k)] & \dots & [Z_{tx}^{rr}(-h,k)] \\ & \vdots & \vdots & \vdots \\ & [Z_{tx}^{rr}(h,-k)] & \dots & [Z_{tx}^{rr}(h,k)] \\ & & & \ddots \end{bmatrix} \tag{50}$$

Then,

$$[\mathbf{Z_t}] = [\mathbf{\Gamma_g}][\mathbf{Z_{tx}}][\mathbf{B_{tx}}] \tag{51}$$

The term λ denotes the transformer effective winding ratio whereas the parameter $[\mathbf{Z_t}]$ is the leakage impedance matrix of the transformer with appropriate adjustment for non-fundamental frequencies. Such adjustment can be found in [32] and [33]. The voltage equation of the delta-grounded wye transformer in (46) is used to augment the rows of the system admittance matrix thus yielding augmented matrix $[Y_{Aug}]$ as in (45). This must be done whilst taking into account the node positions (ie. the 'f' and 'g' nodes where this transformer is located in the network). The columns of the augmented admittance matrix are also augmented with the current descriptive equations (CDEs). For this transformer arrangement, the CDE is written in (52).

$$\begin{vmatrix} [\mathbf{I_{tx}^{fa}}] \\ [\mathbf{I_{tx}^{fb}}] \\ [\mathbf{I_{tx}^{fc}}] \\ [\mathbf{I_{tx}^{ga}}] \\ [\mathbf{I_{tx}^{gb}}] \\ [\mathbf{I_{tx}^{gc}}] \end{vmatrix} = \begin{bmatrix} [\mho] & & -[\mho] \\ -[\mho] & [\mho] & \\ & -[\mho] & [\mho] \\ -[\lambda_r \mho] & & \\ & -[\lambda_y \mho] & \\ & & -[\lambda_b \mho] \end{bmatrix} \begin{vmatrix} [\mathbf{I_{tx}^{ry}}] \\ [\mathbf{I_{tx}^{yb}}] \\ [\mathbf{I_{tx}^{br}}] \end{vmatrix} \tag{52}$$

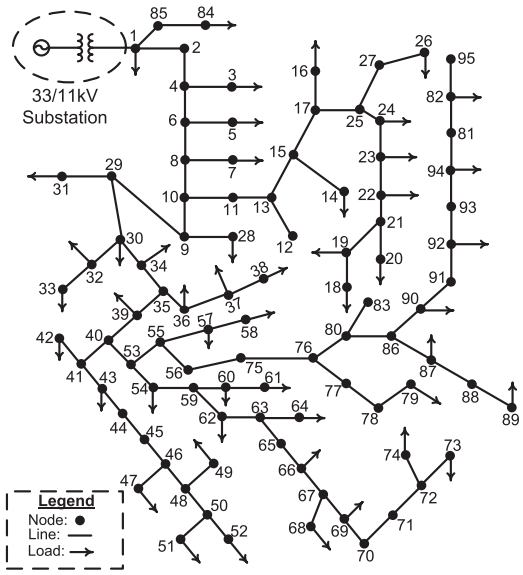

Fig. 4. UKDG 95 bus distribution network.

From the CDEs, the terms $[\mathbf{C}_f]$ and $[\mathbf{C}_g]$ in (45) are given as:

$$[\mathbf{C}_f] = \begin{bmatrix} [\mho] & & -[\mho] \\ -[\mho] & [\mho] & \\ & -[\mho] & [\mho] \end{bmatrix} \tag{53}$$

$$[\mathbf{C}_g = \begin{bmatrix} -[\lambda_r \mho] & & \\ & -[\lambda_y \mho] & \\ & & -[\lambda_b \mho] \end{bmatrix} \tag{54}$$

It is clear that $[\mathbf{C}_f] = [\mathbf{\Gamma}_f]^T$ and $[\mathbf{C}_g] = [\mathbf{\Gamma}_g]^T$. Further theoretical insights into the MNA technique can be seen in [22].

A. Evaluation of Total Technical Losses of Feeders

In this work, attention is given to the feeder technical losses. The total feeder losses can be expressed as (55).

$$\Delta P_{Fdr} = \left(\sum_{nf=1}^{NF} \sum_{\sigma=\{r,y,b,n\}} \left[\sum_{k=-h}^{h} |I_{fdr}^{\sigma}(k)|^2 R_{fdr}^{\sigma}(k) \right] \right) \tag{55}$$

I_σ and R_σ represent the σ-phase current and resistance respectively. k is the index representing the harmonic order. NF denote the total number of feeders in the network.

IV. Simulation

The first simulated network in this study is UKGDS 95-bus which is shown in Fig. 4. This is a medium voltage network [34]. In the simulations, some of the nodes have been modified to include PV clusters and non-linear switching loads which include among others: {1,3,18,19,24,26,32,36,37,43,52,74}. The PV-RDG cluster nodes were selected at random. The network data were obtained from [34]. The load demand profile index plot for 30-minutes annual sample data is plotted in Fig. 5. A zoomed plot of a section of the demand profile index is shown

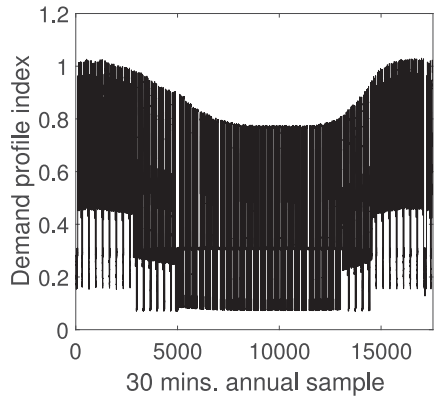

Fig. 5. UKGDS Demand profile index plot for commercial consumer.

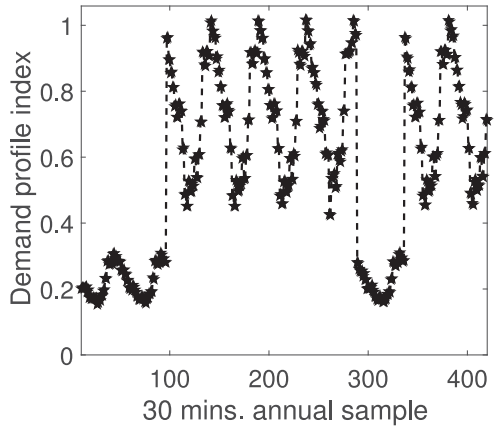

Fig. 6. Zoomed plot of a section of Fig. 5.

in Fig. 6. Note that the demand profile refers to that of urban commercial customers of the UKGDS-95 bus network.

Because this study does not aim to investigate RPF due to PV intermittent generation, a snapshot of the demand profile was used for the simulation; with PV generation considered as a fraction of the load demand. In this way RPF contribution to losses have been isolated, thus allowing for proper quantification of harmonics and unbalanced impacts. Moreover, as mentioned earlier, battery storage systems and optimal sizing of PV-RDG do reduce significantly the impacts of RPF [35] and since this is the trend in recent PV installations, the focus in this work is on harmonics and unbalance loading induced losses.

To study the performance of PV-RDG clusters in a highly unbalanced DN, the standard IEEE-13 bus model has been modified and simulated. The results are also presented and discussed.

For the purpose of validation of results, the simulations have been carried out using the PV harmonic current prediction model presented and the adjusted measured spectra of PV-RDGs provided in [36]. Comparing simulations using the PV model and the measured spectra data reveal the same pattern in the results - i.e. with respect to increase or decrease in feeder losses.

A. Simulation Algorithm

The simulations were realized using a systematic algorithm as shown in the flowchart of Fig. 7. Four scenarios were created by the authors to allow for the comparison of results in relation

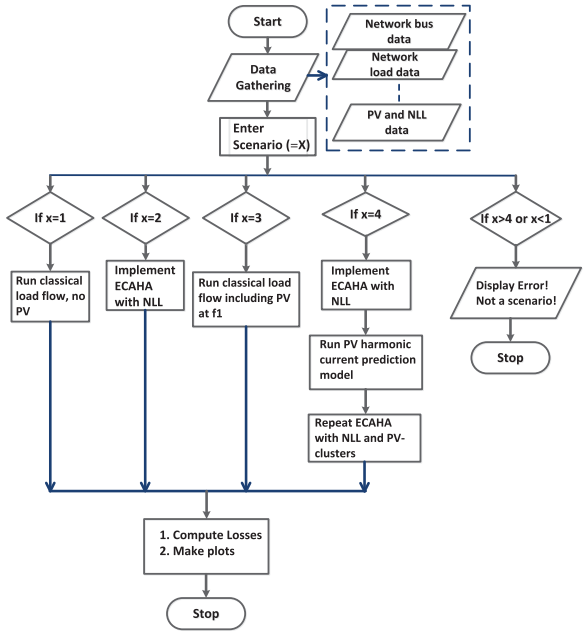

Fig. 7. Flowchart of simulation algorithm.

to the losses evaluated. In the first case, classical load flow analysis similar to [37] was employed and losses calculated. The transformers were modelled as having fixed taps. PV-RDG clusters were considered absent in the network.

The second scenario involved assessing harmonics losses in the network due to significant penetration of NLLs in the system. It was still assumed that the networks in this scenario did not contain PV-RDG clusters. The ECAHA described in earlier sections of this paper have been used for the analysis and the results post-processed to compute losses.

In the third scenario simulation, PV-RDG clusters generating at fundamental frequency were integrated into certain nodes in the network whilst it was assumed that no NLL did exist in the networks. The losses were determined from the post-processed solution variables.

Lastly (scenario 4), it was assumed that NLLs were present in the system. It was also considered that PV-RDG clusters acted as generators both at the fundamental and non-fundamental frequencies. To take into account the network background distortions and its impact on the PV-RDG cluster harmonics performance, the ECAHA was first implemented with NLL alone. Thereafter, the HN-model of the PV-RDG clusters was simulated. This is then integrated into the system with NLL and PV-RDG clusters present and the entire simulation repeated based on the ECAHA approach.

For the scenarios involving NLLs, the spectra data are adjusted. This adjustment is achieved by using the load flow analysis and this is relevant in order to take into account the influence of the network conditions on the NLL harmonics currents. The non-linear loads sepectra data were obtained from [38].

V. Results and Discussions

Although all four scenarios are discussed, only selected results are presented.

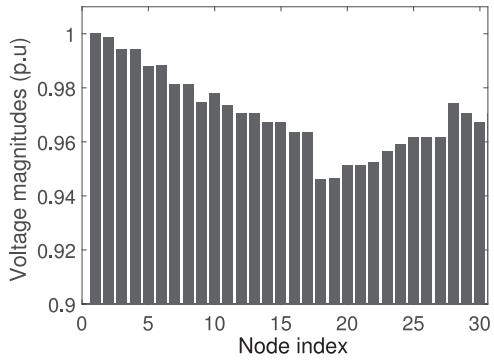

Fig. 8. Selected node voltage magnitude plot for scenario 1.

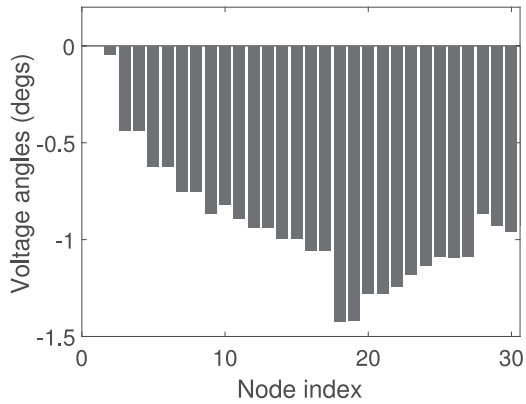

Fig. 9. Selected node voltage phase plot for scenario 1.

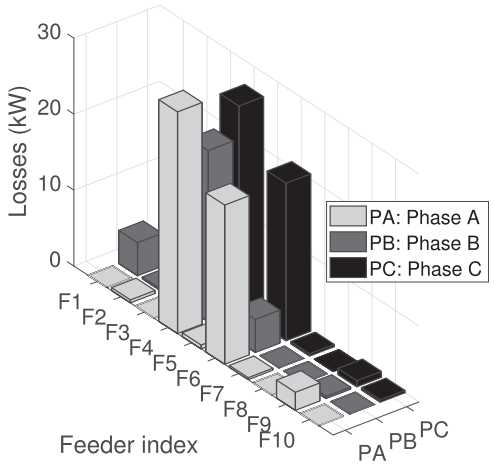

Fig. 10. Per phase per feeder losses for 13-bus model.

A. Scenario 1: No PV-Clusters and Non-Linear Loads in the Network

The calculated total feeder losses for UKGDS-95 bus in this scenario is 92.4 kW.

The least voltage magnitude is at node 18 with a p.u value of 0.95. This is shown in Figs. 8 and 9 where a selected number of node voltage magnitudes and phases have been plotted.

Similarly, a plot of the per-phase per-feeder losses for the modified 13-bus DN is shown in Fig. 10.

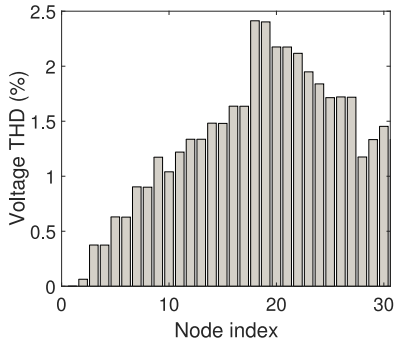

Fig. 11. Voltage THD of selected nodes of UKGDS 95 bus.

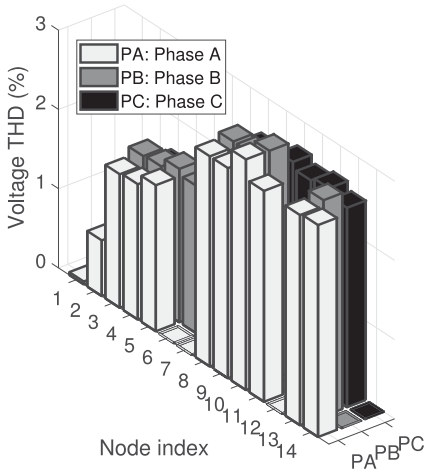

Fig. 12. Voltage THD of modified IEEE 13-bus for scenario 2.

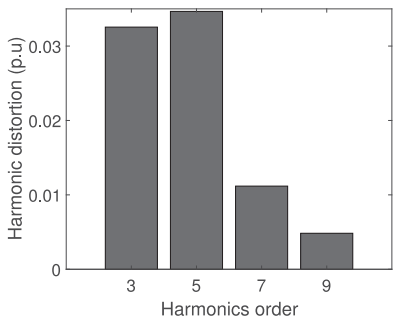

Fig. 13. Plot of selected harmonics spectra.

B. Scenario 2: Network Has Non-Linear Loads but no PV-Clusters

Using the solution variables from the ECAHA algorithm, total losses calculated for the 95-bus model is 99.6 kW. This is equivalent to a loss increase (harmonics induced losses) of 7.2 kW or 7.8% when compared to scenario 1. The voltage THDs for some selected nodes of the 95-bus system and the modified IEEE 13-bus models are shown in Figs. 11 and 12 respectively. The spectra for significant harmonics orders at node 19 is shown in Fig. 13 for completeness. The currents are expressed as per unit (p.u) of the fundamental current. It is clear from the plot that the 5th harmonics current is the most

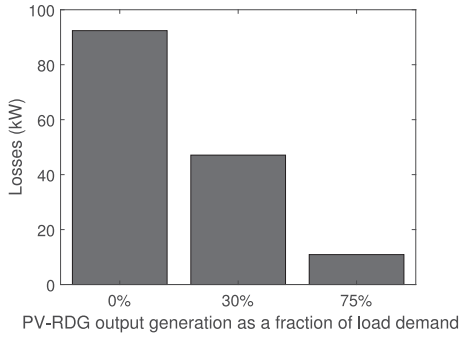

Fig. 14. Plot of losses (kW) as PV-RDG penetration increases - UKGDS 95.

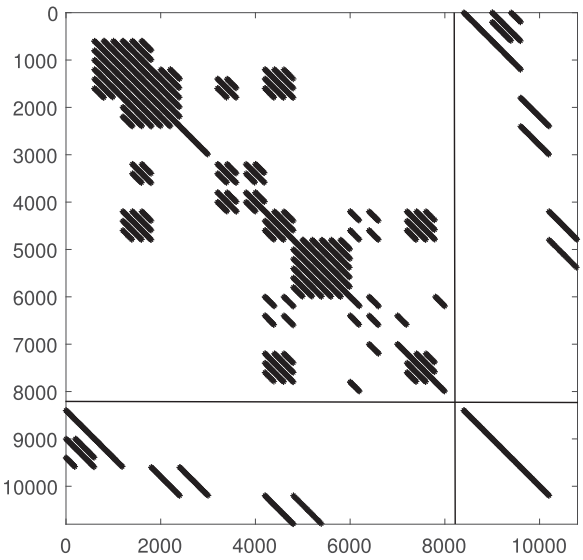

Fig. 15. Augmented admittance matrix plot -modified IEEE-13 bus.

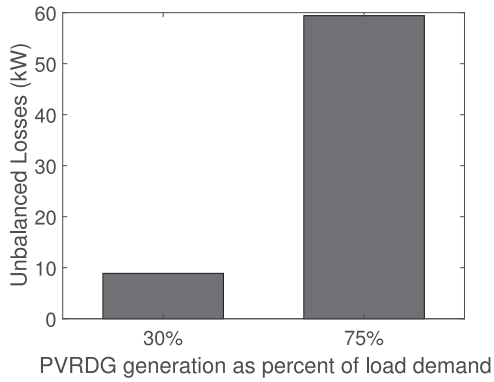

Fig. 16. Plot of losses (kW) induced by further unbalance due to PV-RDG penetration into modified 13-bus model.

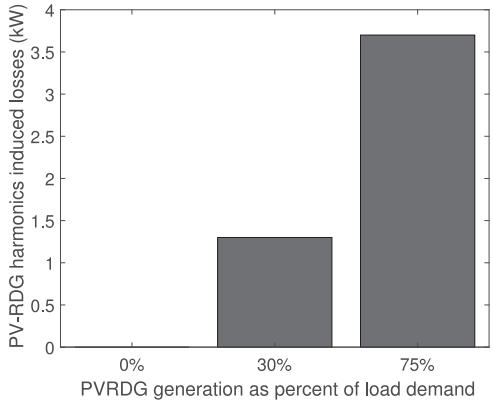

Fig. 17. Plot of PV-RDG harmonics induced losses - modified 13-bus system.

significant. The harmonics induced loss for the modified IEEE 13-bus voltage THD plot shown in Fig. 12 is 0.4 kW and this is only 0.3% of the fundamental losses (obtained from scenario 1 for the same system).

C. Scenario 3: Network has PV Clusters Generating at Only Fundamental Frequency

The third scenario involved assessing the performance of PV clusters in reducing the network losses in the absence of both PV-RDG harmonics and harmonics from the NLLs. The PV clusters generated power have been varied as a fraction of the load demand. The following percentages have been used: $\{0, 30, 75\}\%$. For the 95-bus model, the simulation results revealed a reduction in the feeder losses as the PV-cluster power generation increases. The total losses in the UKGDS 95-bus system when PV-RDG clusters generated 75% of the load demand is 10.9 kW for the UKGD-95 bus (see Fig. 14). This is a loss reduction benefit of 81.5 kW when compared to scenario 1.

For the modified 13-bus system, the augmented admittance matrix sparsity plot is shown in Fig. 15. The simulation results show that optimum PV penetration should be limited to 20% of load demand for the modified 13-bus system. At this level of penetration, the loss reduction benefit is 3.7 kW. Unlike the UKGDS 95 bus, the modified IEEE-13 bus system did not benefit significantly from PV-RDG cluster integration. In fact, the losses increased due to additional unbalance from the PV system integration as plotted in Fig. 16. This shows that integrating PV-RDG in highly unbalanced system might further increase the level of unbalance and thus lead to higher unbalance losses.

D. Scenario 4: PVs Acting as Sources at Both Fundamental and Harmonic Frequencies

Similar to scenario 3, the output powers of the clusters have been varied as $\{0, 30, 75\}\%$ of net load demand at PCC. The simulation results reveal that as PV-cluster penetration increased, the harmonics induced losses also increased for the 95-bus system. The PV-RDG harmonics induced losses for this system during 75% penetration is (3.7 kW) i.e. 4% of the fundamental frequency losses computed in scenario 1. A plot of the PV harmonics-induced losses is shown in Fig. 17. The voltage THD for the above losses computed for the 95-bus system is shown in Fig. 18.

For this system, increasing the PV generation to 100% did not violate the statutory voltage limits of IEEE 519-2014 [39]. However, the PV-RDG harmonics induced losses increased to

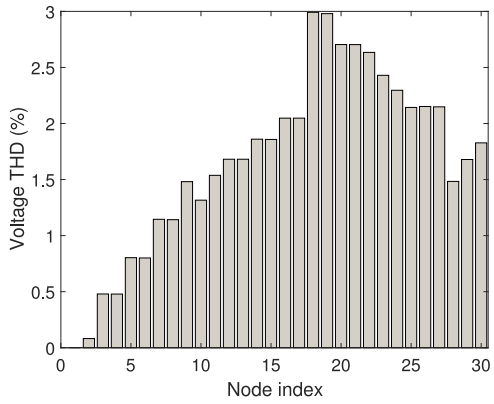

Fig. 18. Plot of voltage THD for selected nodes of UKGDS 95 bus.

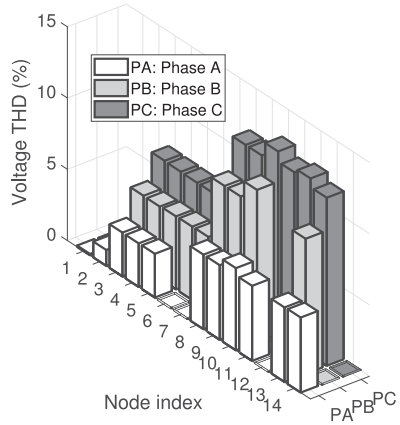

Fig. 20. Plot of voltage THD for modified IEEE 13-bus for 75% case.

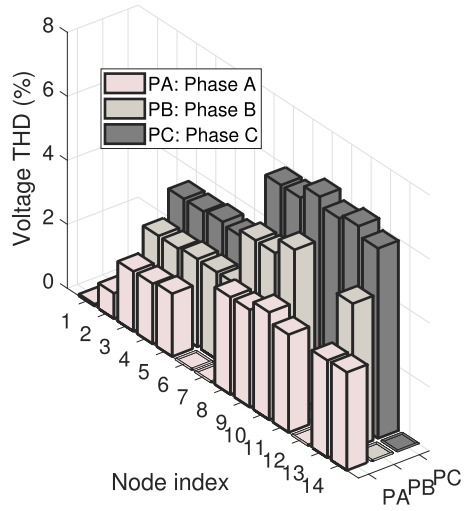

Fig. 19. Plot of voltage THD for modified IEEE 13-bus for 30% case.

5.4 kW thus yielding total harmonics induced losses of 12.6 kW - i.e. including background distortion harmonics losses.

Nevertheless, the induced harmonics loss (3.7 kW) is lesser than the loss reduction benefit (81.5 kW) achieved by the PV-RDG cluster integration in the 95-bus model.

In the case of the modified IEEE 13-bus system, a penetration level exceeding 20% resulted in violation of the standard harmonics limits of IEEE 519-2014 [39]. The voltage THD plots for 30% and 75% cases are illustrated in Figs. 19 and 20. The harmonics losses became very significant as the level of voltage THD increased - though the standard limit was exceeded in such case. It is interesting to point out that Figs. 19 and 20 have the highest THD voltage values experienced in phase 'c' unlike Fig. 12 of scenario 2 which had highest THDs mostly at the phase 'a'. This is expected owing to unbalanced harmonics.

The observation that harmonics can constrain the uptake of higher penetration of PV-RDG clusters is in agreement with previous study [10]. It was also realized that the modified IEEE-13 bus system experienced higher losses due to unbalance than harmonics (i.e. based on simulation results).

VI. Conclusion

The research findings suggest that although PV-RDG cluster integration can reduce losses for some systems, the harmonics and unbalance effects introduced by their presence can challenge the system feeder in terms of higher harmonics and unbalance induced losses and statutory limit violations. The harmonics induced losses increased with increasing node voltage THDs resulting from higher harmonic penetration level from the PV clusters. It was also realized that system parameters, types of loads (electronic or passive load types) and network operating conditions can influence the results.

Furthermore, the research findings reveal that the notion of optimal accommodation of RDGs like PVs without dealing with technical issues like harmonics and unbalance would not necessarily translate to significant loss reduction benefits. Again, tackling only reverse power flows (RPF) and voltage rise issues associated with PV-RDG cluster uptake does not imply feeder relief and hence higher loss reduction benefits for all networks. Technical issues like unbalance and harmonics must be addressed in tandem as these can challenge the system operation like RPF and voltage rise issues.

Appendix

TABLE I
IEEE 519 - 2014 Standard Harmonic Limits [39]

Voltage level V (kV)	Voltage THD (%)	Max. HD (%)
$V \leq 1$	8.0	5.0
$1 < V \leq 69$	5.0	3.0
$69 < V \leq 161$	2.5	1.5
$161 < V$	1.5	1.0

TABLE II
Loading Level of Modified IEEE-13 Bus System

Pa(kW)	Pb(kW)	Pc(kW)	Qa(kVAr)	Qb(kVAr)	Qc(kVAr)
1158	973	1135	606	627	753

TABLE III
LOADING LEVEL OF UKGDS-95 BUS SYSTEM

P(MW)	Q(MVAr)	S(MVA)
3.96	0.96	4.08

REFERENCES

[1] T. Number, "Low carbon networks fund full submission pro-forma," [Online]. Available: https://www.ssepd.co.uk/WorkArea/DownloadAsset.aspx?id=5247. Accessed on: Mar. 5, 2015.

[2] M. Stojkov, K. Trupinic, and S. Nikolovski, "Technical losses in power distribution network," in *Proc. IEEE Mediterranean Electrotech. Conf.*, 2006, pp. 1048–1051.

[3] C. d. Oliveira, N. Kagan, S. Jonathan, S. Caparroz, and J. Cavaretti, "A new method for the computation of technical losses in electrical power distribution systems," in *Proc. 16th Int. Conf. Exhib. Elect. Distrib., Part 1, Contrib (IEE Conf. Publ No. 482)*, 2001, pp. 328–328.

[4] J. R. Agero, "Improving the efficiency of power distribution systems through technical and non-technical losses reduction," in *Proc. IEEE PES Transmiss. Distrib. Conf. Expo.*, 2012, pp. 1–8.

[5] C. A. Dortolina and R. Nadira, "The loss that is unknown is no loss at all: A top-down/bottom-up approach for estimating distribution losses," *IEEE Trans. Power Syst.*, vol. 20, no. 2, pp. 1119–1125, May 2005.

[6] J.-H. Teng and C.-Y. Chang, "Backward/forward sweep-based harmonic analysis method for distribution systems," *IEEE Trans. Power Del.*, vol. 22, no. 3, pp. 1665–1672, Jul. 2007.

[7] K. Balamurugan and D. Srinivasan, "Review of power flow studies on distribution network with distributed generation," in *Proc. IEEE 9th Int. Conf. Power Electron. Drive Syst.*, 2011, pp. 411–417.

[8] L. F. Ochoa and G. P. Harrison, "Minimizing energy losses: Optimal accommodation and smart operation of renewable distributed generation," *IEEE Trans. Power Syst.*, vol. 26, no. 1, pp. 198–205, Feb. 2011.

[9] E. Demirok, D. Sera, R. Teodorescu, P. Rodriguez, and U. Borup, "Clustered PV inverters in LV networks: An overview of impacts and comparison of voltage control strategies," in *Proc. Electrical Power Energy Conf.*, 2009, pp. 1–6.

[10] K. Dartawan, L. Hui, R. Austria, and M. Suehiro, "Harmonics issues that limit solar photovoltaic generation on distribution circuits," in *Proc. World Renewable Energy Forum Colorado Renew. Energy Soc. Annu. Conf.*, 2012, pp. 2292–2298.

[11] D. Gallo *et al.*, "Case studies on large PV plants: Harmonic distortion, unbalance and their effects," in *Proc. Power Energy Soc. General Meet. (PES)*, 2013, pp. 1–5.

[12] O. Nduka and B. Pal, "Harmonic domain modelling of PV system for the assessment of grid integration impact," *IEEE Trans. Sustain. Energy*, vol. 8, no. 3, pp. 1154–1165, Jul. 2017.

[13] O. S. Nduka and B. C. Pal, "Harmonic characterisation model of grid interactive photovoltaic systems," in *Proc. IEEE Int. Conf. Power Syst. Technol.*, 2016, pp. 1–6.

[14] D. Zammit, C. S. Staines, and M. Apap, "Pr current control with harmonic compensation in grid connected PV inverters," *World Acad. Sci., Eng. Technol., Int. J. Elect. Comput. Energetic Electron. Commun. Eng.*, vol. 8, no. 11, pp. 1773–1779, 2014.

[15] D. G. Infield, P. Onions, A. D. Simmons, and G. A. Smith, "Power quality from multiple grid-connected single-phase inverters," *IEEE Trans. Power Del.*, vol. 19, no. 4, pp. 1983–1989, Oct. 2004.

[16] W. Kui, G. Shuhua, H. Qian, H. Yuanhong, and W. Qinfang, "Investigation of harmonic distortion and losses in distribution systems with non-linear loads," in *Proc. China Int. Conf. Elect. Distrib.*, 2008, pp. 1–6.

[17] M. J. Ghorbani and H. Mokhtari, "Impact of harmonics on power quality and losses in power distribution systems," *Int. J. Elect. Comput. Eng.*, vol. 5, no. 1, pp. 166–174, 2015.

[18] C. Lombard and A. Rens, "Evaluation of system losses due to harmonics in medium voltage distribution networks," in *Proc. IEEE Int. Conf. Energy Conf.*, 2016, pp. 1–6.

[19] *IEEE Standard Definitions for the Measurement of Electric Power Quantities Under Sinusoidal, Nonsinusoidal, Balanced, or Unbalanced Conditions*, IEEE Standard 1459-2010, 2010.

[20] M. Madrigal and E. Acha, "A new harmonic power flow method based on the instantaneous power balance," in *Proc. IEEE 10th Int. Conf. Harmonics Quality Power*, 2002, vol. 2, pp. 655–662.

[21] J. Arrillaga, A. Medina, M. Lisboa, M. Cavia, and P. Sanchez, "The harmonic domain. a frame of reference for power system harmonic analysis," *IEEE Trans. Power Syst.*, vol. 10, no. 1, pp. 433–440, Feb. 1995.

[22] T. Noda, A. Semlyen, and R. Iravani, "Entirely harmonic domain calculation of multiphase nonsinusoidal steady state," *IEEE Trans. Power Del.*, vol. 19, no. 3, pp. 1368–1377, Jul. 2004.

[23] W. Kersting, "The whys of distribution system analysis," *IEEE Ind. Appl. Mag.*, vol. 17, no. 5, pp. 59–65, Sep./Oct. 2011.

[24] R. Burch *et al.*, "Impact of aggregate linear load modeling on harmonic analysis: A comparison of common practice and analytical models," *IEEE Trans. Power Del.*, vol. 18, no. 2, pp. 625–630, Apr. 2003.

[25] N. R. Watson, T. L. Scott, and S. J. Hirsch, "Implications for distribution networks of high penetration of compact fluorescent lamps," *IEEE Trans. Power Del.*, vol. 24, no. 3, pp. 1521–1528, Jul. 2009.

[26] "Call for innovation ideas, uk power networks," 2014. [Online]. Available: https://www.becbusinesscluster.co.uk/images/uploads/notice-board/Call-for-Innovation-Ideas-on-behalf-of-UK-Power-Networks.pdf. Accessed on: Mar. 5, 2015.

[27] S. Daniel, "Distributed (home) energy storage and aggregated grid services," 2016. [Online]. Available: http://www.energy.ox.ac.uk/wordpress/wp-content/uploads/2016/12/Daniel- Moixa.pdf

[28] N. T. M. Dale, R. Hey, and P. Swift, "Project sola bristol, closedown report, western power distribution," 2016. [Online]. https://www.westernpower.co.uk/docs/Innovation/Closed-projects/SoLa-Bristol/SoLa-Bristol-Closedown-Report-FINAL-090616-CLEAN.aspx

[29] P. Siano and G. Mokryani, "Probabilistic assessment of the impact of wind energy integration into distribution networks," *IEEE Trans. Power Syst.*, vol. 28, no. 4, pp. 4209–4217, Nov. 2013.

[30] H. Hu, Q. Shi, Z. He, J. He, and S. Gao, "Potential harmonic resonance impacts of PV inverter filters on distribution systems," *IEEE Trans. Sustain. Energy*, vol. 6, no. 1, pp. 151–161, Jan. 2015.

[31] J. Vlach and K. Singhal, *Computer Methods for Circuit Analysis and Design*. Berlin, Germany: Springer Science and Business Media, 1983.

[32] E. Acha and M. Madrigal, *Power Systems Harmonics*. Hoboken, NJ, USA: Wiley, 2001.

[33] T. Densem, P. Bodger, and J. Arrillaga, "Three phase transmission system modelling for harmonic penetration studies," *IEEE Trans. Power Apparatus Syst.*, vol. PAS-103, no. 2, pp. 310–317, Feb. 1984.

[34] R. Singh, "State estimation in power distribution network operation," Ph.D. dissertation, Control and Power Research Division, Electrical and Electronic Engineering Department, Imperial College London, London, 2009.

[35] M. J. Alam, K. Muttaqi, and D. Sutanto, "A three-phase power flow approach for integrated 3-wire MV and 4-wire multigrounded LV networks with rooftop solar PV," *IEEE Trans. Power Syst.*, vol. 28, no. 2, pp. 1728–1737, May 2013.

[36] E. C. Aprilia, "Modelling of photovoltaic (PV) inverter for power quality studies," M.S. thesis, Electrical Engineering, Technische Universiteit Eindhoven Univ. Technol., Eindhoven, 2012.

[37] I. Kocar, J. Mahseredjian, U. Karaagac, G. Soykan, and O. Saad, "Multiphase load-flow solution for large-scale distribution systems using MANA," *IEEE Trans. Power Del.*, vol. 29, no. 2, pp. 908–915, Apr. 2014.

[38] R. Burch *et al.*, "Test systems for harmonics modeling and simulation," *IEEE Trans. Power Del.*, vol. 14, no. 2, pp. 579–587, Apr. 1999.

[39] *IEEE Recommended Practice and Requirements for Harmonic Control in Electric Power Systems*, IEEE Standard 519-2014, 2014.

Authors' photograph and biography not available at the time of publication.